

Freezing Nucleation Rates of Dilute Solution Droplets Measured between -30° and -40°C in Laboratory Simulations of Natural Clouds

PAUL J. DEMOTT AND DAVID C. ROGERS

Department of Atmospheric Science, Colorado State University, Fort Collins, Colorado

(Manuscript received 20 April 1989, in final form 3 November 1989)

ABSTRACT

A 1.2 m^3 continuous slow-expansion cloud chamber was used to simulate natural, liquid cloud formation on soluble cloud condensation nuclei (CCN). Droplet freezing was observed during continued simulated adiabatic ascent and cooling to -40°C . Sharply increasing ice nucleation rates were observed between -34° and -39°C , independent of the chemical composition of three CCN used. From the experimental data, nucleation rates are estimated assuming a homogeneous-freezing mechanism. It is concluded that homogeneous-freezing was observed. The results are compared to other laboratory and field studies. These results compare most closely with values calculated from data taken in real clouds and should be relevant to ice formation in cirrus clouds.

1. Introduction

In the atmosphere, cloud droplets typically freeze as the result of a heterogeneous nucleation process. However, when ice nucleating aerosols are scarce, cloud droplets may supercool to temperatures of -35°C or colder, and nucleation of ice may ultimately occur homogeneously in solution droplets. Spontaneous freezing has been treated by fluctuation theory (e.g., Pruppacher and Klett 1978; Heymsfield and Sabin 1989), and has been studied in the laboratory (Pruppacher and Klett 1978; Butorin and Skripov 1972; Hagen et al. 1981; Taborek 1985) and in the atmosphere (Sassen and Dodd 1988). Theory predicts that the homogeneous nucleation rate in water drops J_{ls} ($\text{cm}^{-3}\text{ s}^{-1}$) increases sharply with decreasing temperature. Experimental estimates of J_{ls} versus temperature have been derived from laboratory studies that utilized a variety of techniques, most of which required that artificially prepared droplets or emulsions be supported, in a medium other than air. Experimental values for suspended droplets summarized by Butorin and Skripov agree reasonably well with Taborek's results for emulsions, but are about 10^2 higher than theoretical values given by Pruppacher and Klett. Hagen et al. studied the freezing of very small and freely suspended pure water droplets produced by rapid expansion of humid air to temperatures below -40°C . Their extrapolation of J_{ls} to temperatures warmer than -40°C gave values as much as 10^9 higher than theory. Sassen and Dodd used in situ and polarization lidar observations in cirrus clouds and comparisons to a numerical model to es-

timate J_{ls} as approximately 10^6 times higher at -35°C than theory. They noted the discrepancy with laboratory results. However, no experimental data have been obtained from which J_{ls} can be estimated for droplets formed naturally in air on CCN under simulated, realistic atmospheric conditions. The studies reported here were conducted to provide this information.

This paper describes simulations that were performed in the Colorado State University dynamic (controlled-expansion) cloud chamber. Our experiments examined the freezing of large populations (on the order of 10^8) of freely suspended cloud droplets of varying concentrations, sizes, and initial CCN chemistry as temperature and pressure were lowered. Aqueous solution droplets formed during the simulated slow-adiabatic expansion-cooling of an air parcel. Ice nucleation rates were estimated and are compared to selected results from earlier studies.

2. Experimental design

a. Instrumentation and related considerations

The basic characteristics of the CSU dynamic cloud chamber in the configuration used for these experiments have been described by DeMott (1988). Additional details are provided here. A cross-section of the chamber is shown in Fig. 1. The chamber consists of a 1.2 m^3 test volume inside a perforated (with small holes) cylindrical copper chamber; wall temperature effects are minimized by circulating temperature controlled fluid through copper tubing that is soldered to the wall. The copper cylinder is enclosed by a thermally insulated stainless steel pressure vessel of 2 m^3 volume. This volume is evacuated to simulate adiabatic cooling.

Corresponding author address: Paul J. DeMott, Dept. of Atmospheric Science, Colorado State University, Fort Collins, CO 80523.

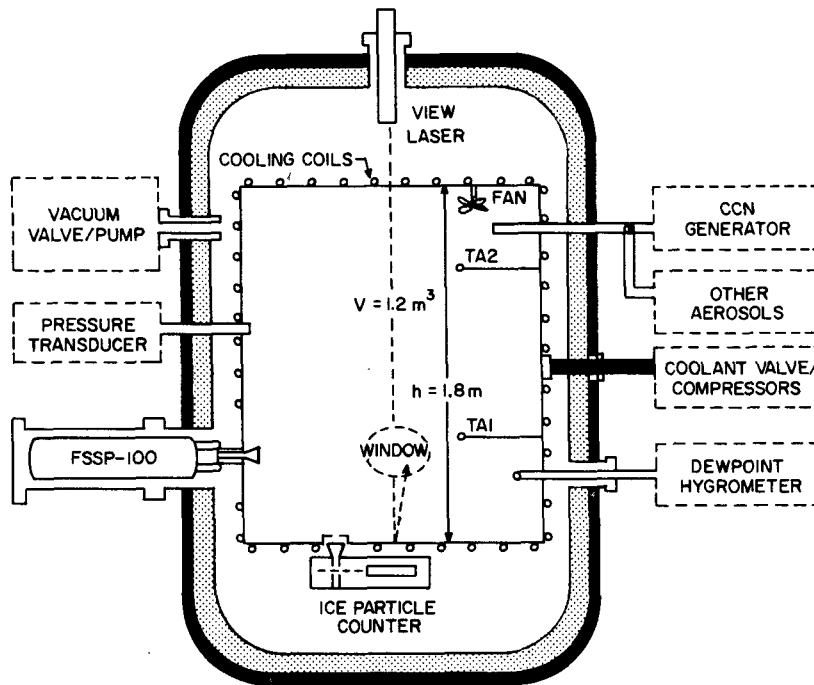


FIG. 1. Schematic diagram of CSU-controlled expansion (dynamic) cloud chamber, as configured for this study. See text for details.

The temperature of the copper cylinder is controlled to match the adiabatic expansion-cooling of the air. Evacuation control, temperature control, and data acquisition are done by microcomputer. Data are recorded at 15 s intervals. Pressure and temperature control are based on equations for dry and moist adiabatic expansion. Air temperature, pressure, humidity, cloud droplet sizes and concentrations, and ice crystal numbers settling from the volume are measured in time.

Temperature is measured continuously using an array of ten copper-Constantan thermocouples (0.508 mm wire) located on the inner liner and two faster response (0.0254 mm wire) thermocouples (TA1, TA2 in Fig. 1) located 25 cm into the air volume from the inner wall. Temperature uncertainty is 0.2°C. Pressure is measured with a strain gauge-type transducer. Sensitivity is 0.5 mb at room pressure (~ 850 mb). Humidity is measured with two optical condensation-type dewpoint hygrometers.

Cloud droplet sizes and concentrations are measured with a Particle Measuring Systems (PMS) FSSP-100. A small funnel shaped glass tube protrudes 10 cm into the cloud volume and draws cloud air into the FSSP. The sample inlet necks down to 0.65 mm, and with a sampling rate of 0.4 L min^{-1} , the flow accelerates to 20 m s^{-1} . This stream is combined with an isokinetic sheath flow and is directed through the center of the laser beam. This sampling system has a number of advantages and avoids some of the measurement problems associated with these instruments when they sample the free air-stream from aircraft (Dye and

Baumgardner 1984; Baumgardner et al. 1985; Cooper 1988). The sample volume in our FSSP system is determined by the size of the laser beam (constant ~ 0.2 mm), the depth of field (DOF), and the air speed (constant). In aircraft FSSP systems, the DOF and the air speed can vary: the DOF is determined with a combination of optics and electronics and is typically 2 to 3 mm. With an FSSP sampling in the free stream, there are many droplets outside the DOF, and they can produce significant coincidence errors in the droplet-size measurements (Cooper 1988). However, in our system, the DOF is defined by the size of the airstream (0.65 mm) carrying the droplets. This air stream is centered in the optical DOF; there are no droplets outside the DOF. The isokinetic sheath flow keeps the edges of the droplet stream intact. This was verified with smoke tests. The particle stream velocity is higher than the minimum required, yet is well below the velocity where size corrections become necessary for this factor (Cerni 1983). At the same time, the volume sample rate of approximately $1 \text{ cm}^3 \text{ s}^{-1}$ results in particle transit rates of 1 to 10^3 s^{-1} in most experiments, well below the 10^5 s^{-1} value for which coincidence errors become important to measuring concentrations (Dye and Baumgardner 1984; Baumgardner et al. 1985; Cooper 1988). There are unavoidable, inherent sizing uncertainties for all FSSP probes which particularly occur in the 1 to $10 \mu\text{m}$ range of particle sizes due to the behavior of the Mie scattering function there (Pinnick and Auvermann 1979). Multiple Mie peaks for droplets below $10 \mu\text{m}$ can lead to uncertainties as

large as a factor of 2 to 3 in diameter. The uncertainty introduced for the clouds measured and calculations made in this study are discussed further in the next section.

Ice crystals are detected by a laser-based detection device similar to that of Lawson and Stewart (1983). A primary difference, however, is that the instrument described by Lawson and Stewart uses transmission/depolarization to detect ice crystals and rolls off to near zero response for particles smaller than about $75 \mu\text{m}$. Our device was configured, instead, to detect single particles by extinction in a laser beam. Ice crystals which fall through a 3.8 mm diameter hole on the bottom of the copper liner are collected by a converging air stream which flows into a funnel-shaped glass sample tube (10 mm o.d. inlet, 0.7 mm o.d. outlet, flow $15 \text{ cm}^3 \text{ s}^{-1}$). This air stream crosses a HeNe laser beam (0.7 mm diameter), which falls on a fast-response solid-state photo detector. The extinction signal should be approximately proportional to the particle cross section area. Experiments have shown that the technique responds to cloud droplets, ice particles, and electronic noise. A threshold circuit is used to discriminate against both noise and small cloud droplets. Cloud droplets rarely reach sizes larger than 20 to $25 \mu\text{m}$ before settling out of the chamber, so the threshold is first calibrated coarsely to detect glass beads of $35 \mu\text{m}$ but not $15 \mu\text{m}$; finer adjustments are made to discriminate against droplets in warm cloud formation tests. The largest droplets in the experiments described here were $15 \mu\text{m}$, so it is unlikely that cloud droplets were mistaken for ice particles. Other evidence also supports this conclusion (i.e., the FSSP measurements collected simultaneously with ice formation). Calibration of the ice particle counts was made versus "ground truth" collections onto microscope slides. From numerous calibrations, it was found that the standard deviation in ice particle counts was about 30% of the total, independent of temperature or ice crystal habit. The total ice-crystal number settled from the chamber was determined by multiplying the ice-particle count by the ratio of liner bottom-surface area to the sample hole area.

A slight measurement lag in detecting freshly nucleated ice crystals occurs because crystals must grow and settle to the bottom of the chamber. "Instantaneous" pulse nucleation tests in the chamber using liquid CO_2 and dry ice injections into supercooled water clouds have shown a nearly Gaussian response, peaking 30 to 75 s after nucleation, depending on temperature and pressure (which affect crystal growth rate and fall velocity). A deconvolution procedure is used to obtain the true response from the measured ice crystal signal (Mage and Noghrey 1972). The finite difference approximation to the Laplace transform that describes the relation between the measured ice crystal signal $s^{-1}(R)$ and the actual nucleation response (X) is given by,

$$R(t) = \sum_{n=1}^{n=\tau/\Delta t} C(n)X(t-n\Delta t)\Delta t \quad (1)$$

where the coefficients $C(n)$ represent a transfer function describing the response to a unit impulse of ice crystals, τ is the total time required for the unit impulse to settle from the chamber, and Δt is a small increment of time. The transfer function for the procedure in this paper is based on pulse nucleation results in the -7 to -12°C temperature range. The ice crystal signal for a particular pulse nucleation test and the transfer-function fit to the data from several of these experiments are shown in Fig. 2. The results of using the procedure on experimental data ($\Delta t = 15 \text{ s}$) are shown later. The transfer function has not been exactly determined for the crystals and conditions existing at homogeneous-freezing temperatures. The use of the warmer temperature transfer function is justified since crystal fall speeds are similar at the colder temperatures and lower pressures. In order to assess the significance in deconvoluting the data, we used the crystal growth and fall equations of Rogers and Vali (1987) to estimate how long it takes for growing crystals to fall out of the chamber. For example, let us hypothesize two droplets that bracket the extremes of observed size, $1 \mu\text{m}$ and $15 \mu\text{m}$ diameter. Let these droplets freeze at -35°C and 400 mb at the top of the chamber. They then grow and sediment in a water-saturated environment. The $15 \mu\text{m}$ droplet falls 180 cm to the bottom of the chamber 84 s later as a solid ice column $32 \mu\text{m}$ long (the change from spherical to columnar habit is assumed to occur at $20 \mu\text{m}$). The $1 \mu\text{m}$ droplet takes 108 s and is also $32 \mu\text{m}$ long. If these droplets start from the middle of the chamber, the fall times are 55 and 78 s , and the crystal lengths at the bottom are 26 and $25 \mu\text{m}$. These model results suggest that the crystals should be

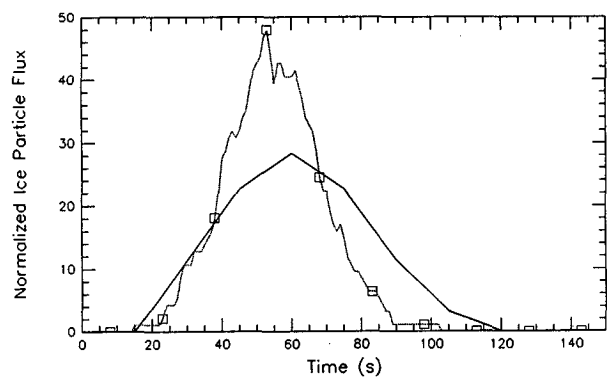


FIG. 2. Normalized response of ice particle counter to seeding a supercooled water cloud at -12°C with a short burst of liquid CO_2 : measurements at 15 s intervals (open squares) and smoothed measurements at 1 s intervals (dotted line). The solid line shows the mathematical function which approximates the response, evaluated at 15 s intervals. The mathematical function is based on this and several other tests.

of detectable size, and if they all nucleated at once, they should be detected between about 55 and 110 s. These are similar to the times for crystal growth and sedimentation in the warmer temperature region where the transfer function was defined. At this time, we do not have observations of the crystal sizes or habits in the cloud chamber, although we are installing a microscope video camera to provide this information in the future.

There are clearly uncertainties in trying to deconvolute the ice-particle flux data. If we do not perform the deconvolution, there will be two effects: the estimates of nucleation temperature will be too cold, and the calculations of J_{is} will be too small. The maximum possible error in nucleation temperature can be estimated from the cooling rate, which is about $1.0^{\circ}\text{C min}^{-1}$ for a 2.5 m s^{-1} updraft. From the model calculations and from the liquid CO_2 tests, the time lag between nucleation and the first detection of ice is 30 to 60 s, so the temperature error in nondeconvoluted data will be about 0.5 to 1.0°C . It is more difficult to estimate the error in J_{is} because the exact duration of nucleation (for liquid CO_2 injections) is unknown. If we estimate this duration as about 2 s, then the error in J_{is} could be as large as a factor of 15 (the width of the transfer function, 30 s divided by 2 s). It is important to deconvolute the data, although the results will not be drastically different if we do not (values of J_{is} range over five orders of magnitude in our experiments). We are investigating other methods for performing this mathematical correction and for detecting the nucleation.

In these experiments, a water cloud is quickly transformed (over a few minutes) to an ice cloud, so as supersaturations drop, cloud drops begin to evaporate and further ice particle growth is eventually inhibited. Consequently, at some point during cloud glaciation the transfer function is no longer valid, since ice growth rates are inhibited. Therefore, the calculations of nucleation rates were not carried out beyond the point where cloud droplet concentrations fell below about 50 cm^{-3} . Still, it can be expected that the deconvolution procedure we used may underestimate the nucleation rate at the coldest temperatures calculated because crystal growth slowed in response to lowered saturation ratio.

b. Procedures

In order to avoid possible effects of impurities on nucleation, the cloud chamber surfaces and sample lines were carefully cleaned at the start of the experimental series. Initial conditions for these experiments used ambient pressure (840 mb) and temperature ($+20^{\circ}\text{C}$) air with initial dewpoints between -15°C and -25°C , and particle concentrations $< 0.1 \text{ cm}^{-3}$ as measured by a condensation nucleus (CN) counter (Thermo Systems Inc., Model 3020). Peak supersaturation of butanol achieved in the CN counter is

$\sim 300\%$, so concentrations are considered to be the Aitken particle concentrations. The simulated adiabatic expansion rate was standardized to 2.5 m s^{-1} ($\sim 1^{\circ}\text{C min}^{-1}$ cooling) in all experiments. With these conditions, cloud formation occurred between -20°C and -30°C . The expansions continued until the temperature fell to $< -40^{\circ}\text{C}$.

CCN were generated by bubbling filtered dry air through 1% (by weight) solutions of either ammonium sulfate, ammonium bisulfate, or sodium chloride in doubly distilled and deionized water. These CCN aerosols were polydisperse, having modal diameters near $0.1 \mu\text{m}$, and concentrations at the start of expansion were 1000 to 1500 cm^{-3} . Concentrations of particles produced from bubbling the distilled water with no dissolved salt were nearly three orders of magnitude lower. These particles could have contaminated the experiments by acting as heterogeneous ice nuclei, although the cumulative numbers of ice crystals that formed in the experiments were far too large ($\sim 10^8$) to be explained by these few insoluble particles ($\sim 10^5$). Another source for heterogeneous ice nuclei was the insoluble trace material in the reagent grade soluble salts used for CCN generation. Pruppacher and Neiberger (1963) found "large" but unspecified quantities of insoluble particles in solutions made with highly purified water, and noted the potential effect on freezing of highly supercooled solutions. Manufacturer-specified insoluble content of the salts used in our experiments was $< 0.002\%$ (J. T. Baker Chemical Co., reagent grade). At this level, it is possible that every soluble CCN particle generated could *potentially* contain one $\sim 0.01 \mu\text{m}$ diameter insoluble particle, although it seems highly unlikely that the insoluble material would be distributed in this manner. It can only be noted that some potential for heterogeneous contamination existed. However, other experimental results following contamination by heterogeneous aerosols, and following the purposeful use of particles of high insoluble content as CCN (DeMott 1989) support our assumption that the trace insoluble material had little or no influence on the results presented here, particularly below -34°C . This is discussed later in this paper. Salt concentrations in nucleated droplets were less than 10^{-3} molar, which should have no influence on freezing temperature, except during cloud evaporation at glaciation.

Up to the point of total cloud glaciation, it was possible to calculate the homogeneous-freezing nucleation rate J_{is} ($\text{cm}^{-3} \text{ s}^{-1}$) from the numbers of ice crystals formed during discrete time intervals, from cloud droplet concentration, and from average droplet diameter. That is,

$$J_{is} \approx \frac{X_i}{(V_d N_d V_c)} \quad (2)$$

where X_i is the instantaneous rate of ice crystal formation (number s^{-1}) from (1), V_c is chamber volume, and V_d and N_d are average droplet volume and droplet concentration, respectively. Equation (1) was applied at each 15 s data record. This equation is strictly valid for monodisperse droplets, but it should be appropriate for large populations of dispersed cloud droplets if the size distribution is peaked in a narrow range of sizes about the mean. Uncertainties involved are discussed in relation to the presentation of experimental data in section 3.

3. Results

Data from a homogeneous freezing experiment (ammonium sulfate CCN) are shown in Figs. 3 and 4. Figure 3 shows time, temperature, cloud droplet con-

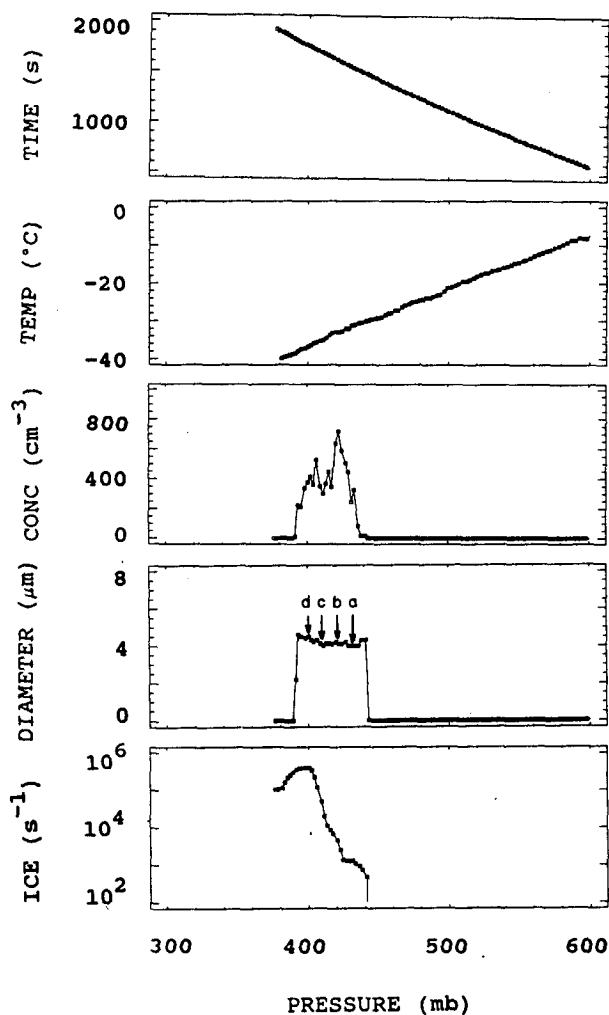


FIG. 3. Plots of time, temperature, droplet concentration, average droplet diameter, and ice crystals formed s^{-1} as a function of pressure during a simulated adiabatic expansion. Simulated updraft was 2.5 m s^{-1} . Letters (a, b, c, d) refer to points where droplet spectra are presented in Fig. 5.

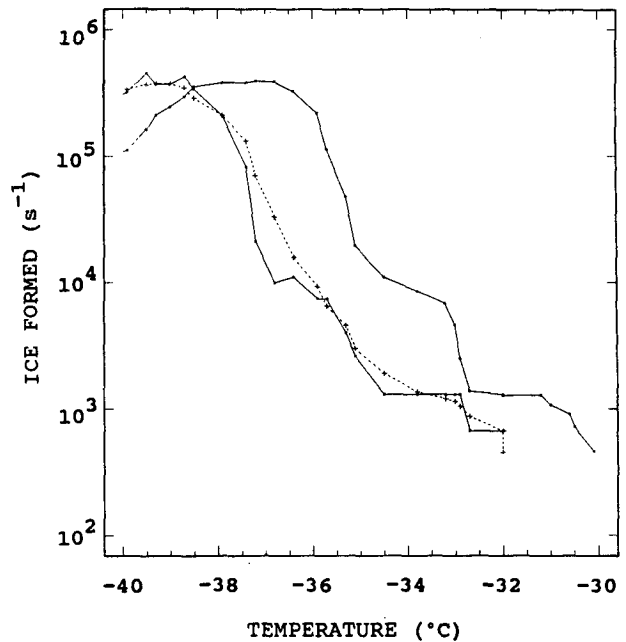


FIG. 4. Instantaneous raw (—●—), smoothed raw (—+—), and deconvoluted (top curve) numbers of ice crystals formed, plotted as a function of temperature. The experiment shown is the same as in Fig. 3.

centration, average droplet diameter and ice crystals formed s^{-1} (computed at 15 s intervals) during a portion of the simulation of adiabatic cooling and expansion. Cloud droplet size spectra at selected points are shown in Fig. 5. Figure 4 shows the instantaneous number of ice crystals formed as a function of temperature for the same experiment. The raw signal is distinguished from the deconvoluted signal to show the effect of the application of the transfer function described in section 2. The raw signal was smoothed with a binomial filter to prevent numerical instabilities in using (1). Notice that ice formation began in this particular experiment with cloud formation near -30°C , and generally increased rapidly in rate until complete cloud glaciation near -38.5°C (395 mb in Fig. 3).

Initially, nine such experiments were performed. Droplet concentrations ranged from 50 to 700 cm^{-3} , and average droplet diameters ranged from 3 to 7 μm at the onset of freezing. The cloud droplet size distributions were characterized by dispersion values near 0.3. The point of cloud glaciation is quite apparent in Fig. 3. Note that the water cloud rapidly evaporates after the ice crystal formation rate exceeds $\sim 3 \times 10^6 \text{ s}^{-1}$. For all experiments together, the temperature at which cloud rapidly dissipated was $-37.5 \pm 0.4^\circ\text{C}$. The cumulative number of ice crystals formed by -40°C in Fig. 4 is about 30% of the total number of droplets originally present; this result was typical ($\pm 20\%$). The remaining 70% of droplets evaporated. Once rapid gla-

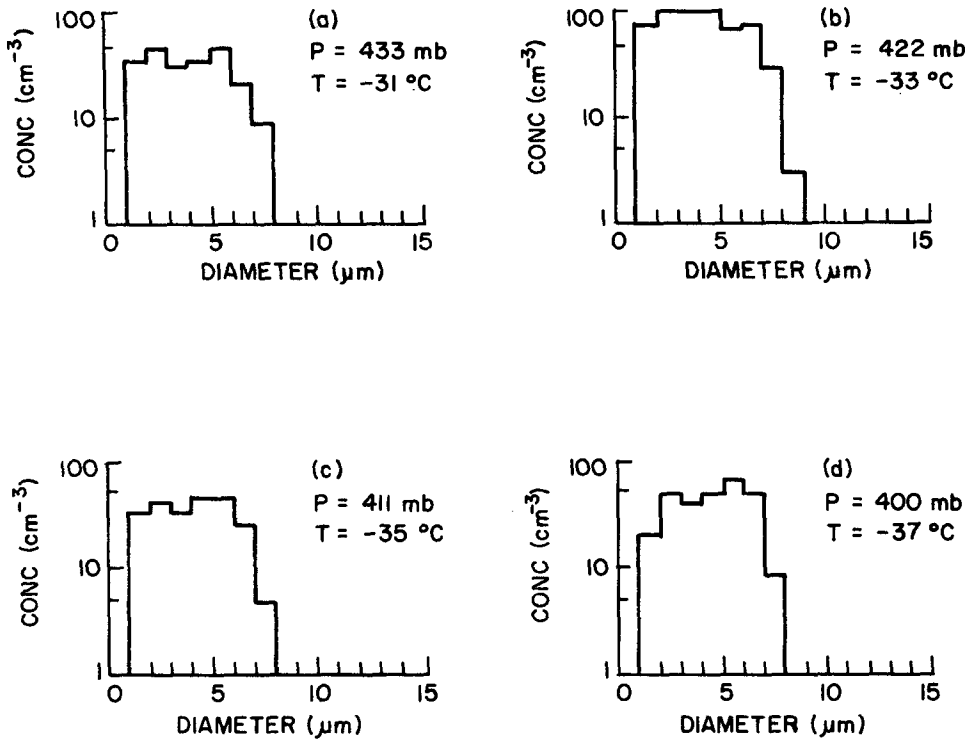


FIG. 5. FSSP cloud droplet size spectra at various points (a, b, c, d) in the experiment shown in Fig. 3.

ciation began, the experiments lost sensitivity to detect further ice nucleation. It was thus not possible to calculate a median droplet freezing temperature—a parameter used to characterize the results of many earlier laboratory studies reported in the literature.

The temperature range in which J_{is} can be estimated from the data is approximately -32.5° to -38.5°C . The results of the computations for the experiment shown in Figs. 3 and 4 are shown in Fig. 6. Again, the result without deconvolution is displayed to indicate the effect and importance of the procedure to the results. The results shown in Fig. 6 are typical of all nine experiments, for any one of the three CCN chemistries we used. No significant or systematic difference in the temperature dependence of J_{is} was found as a function of CCN chemistry. This result was as expected since the aqueous solutions present in cloud droplets are quite dilute ($<10^{-3}$ molar). Results of all tests are therefore presented together as a single sample scatterplot in Fig. 7. Typical J_{is} values measured were 5×10^5 at -35°C and 5×10^7 at -37°C . Greater spread in values is noted at temperatures warmer than about -34°C —which may be a sign of contamination by the small amounts of insoluble matter than may be introduced with CCN particles—and below -37°C , where rapid cloud changes due to increasing ice formation affected the computations.

The uncertainty in calculated values of J_{is} can be estimated from uncertainties in measurements of

droplet size and concentration, and ice crystal detection. As discussed, X_i has an associated uncertainty of 30%. Average droplet diameter uncertainty is taken as



FIG. 6. Computed nucleation rate J_{is} ($\text{cm}^{-3} \text{s}^{-1}$) as a function of temperature for the experiment shown in Fig. 3. The lower curve is from the raw ice signal. The upper is from the true (deconvoluted) signal.

a factor of 2 to account for the inherent ambiguity of the FSSP sizing of drops smaller than $10\ \mu\text{m}$. Short-term temporal changes of up to 30% in N_d are evident in Fig. 3 and may indicate spatial inhomogeneities of the same magnitude throughout the chamber. The greatest uncertainty contribution is from the sizing of cloud droplets. Using these uncertainties in (2), and standard error propagation methods, we estimate the uncertainty in J_{fs} is a factor of 6. This is consistent with the spread of calculated values in Fig. 7.

It is our assertion that the results in Fig. 7 represent homogeneous-freezing nucleation rates at temperatures below -34°C . This is supported by other experiments we did, where heterogeneous contamination occurred (purposely in one case and accidentally in the other). We present these other data here for comparison. Figure 8 shows the results from the initial experiments (indicated by points coded as $\underline{1}$'s) compared to the results for six soluble "CCN only" experiments [which were performed after a large series of heterogeneous ice nucleation experiments using carbonaceous soot in the chamber, ($\underline{2}$)], and three experiments in which carbonaceous soot particles were forced to act as CCN

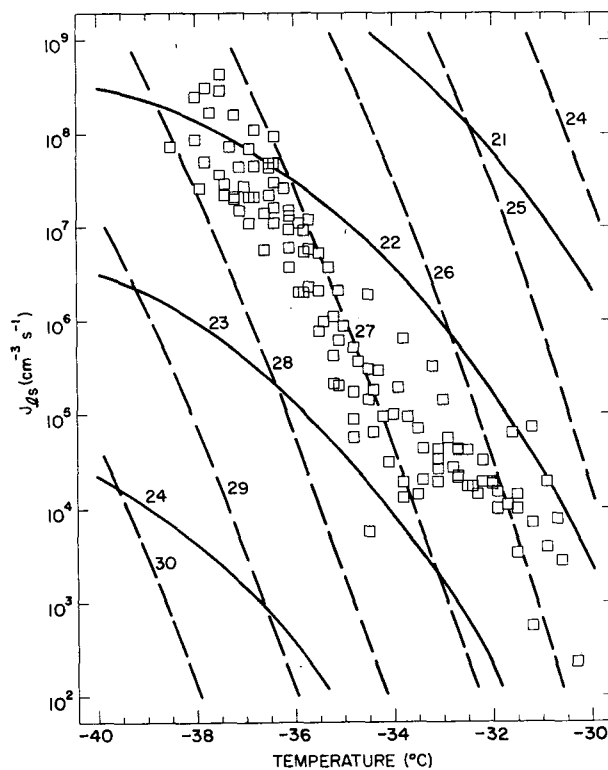


FIG. 7. Summary of results for nucleation rate versus temperature in nine experiments with three CCN types (\square). Theoretical homogeneous freezing nucleation rates are shown by solid and dashed curves denoting various assumed values of interfacial surface tension σ_{i-w} (ergs cm^{-2}). Solid and dashed curves of σ_{i-w} assume temperature dependent and constant values, respectively, for the quantities L_f and ΔF_{act} , as described in the text.

($\underline{3}$). The latter experiments are reported by DeMott (1990). The other CCN experiments were originally intended to add to the sample size for the study reported here, but the sample inlet piping was obviously contaminated by the soot experiments. The effect of heterogeneous nucleation can be seen by comparing the contaminated results with the initial soluble CCN series. Note that the results from all three converge at temperatures below -34°C . Warmer than -32°C , the nucleation rate shows little dependence on temperature. Colder than -32°C , the rate increases rapidly and consistently. This change in rate strongly suggests a change in the mechanism responsible for ice formation. The limiting (competing) rate at the coldest temperatures is the homogeneous rate; it shows no preference for the absence or presence of the inert soot particles in the drops.

The experimental results obtained in this study are compared with the results of other experimental studies in Fig. 9. Uncertainties in J_{fs} (vertical lines) and temperature (horizontal capping lines) are indicated by error bars in our experimental results. The slope of the results for homogeneous freezing nucleation rate in all studies are similar, but our J_{fs} are 10^1 to 10^3 higher than Butorin and Skripov (1972) for prepared distilled water droplets, and more than 10^3 lower than results extrapolated for pure water droplets formed by rapid expansion in the experiments of Hagen et al. (1981). The calculations of Sassen and Dodd (1988), based on observations in real clouds, fall within an order of magnitude on the high side of our results. It is not obvious why Butorin and Skripov's purified water droplets supported in oil or Taborek's emulsions should freeze at colder temperatures than freely suspended dilute solution droplets.

The results for theoretical nucleation rate are also compared to our results in Fig. 9. The experimental rate exceeded the theoretical rate by 10^3 to 10^5 over the temperature range from -34° to -37°C . It is useful to ask what the values of critical theoretical parameters would have to be to provide agreement with our experimental results. After all, the classical theoretical rates shown in Fig. 9 include assumptions concerning the interfacial surface tension at the ice-water interface in a supercooled droplet (σ_{i-w}), the activation energy for self-diffusion (ΔF_{act}), and the appropriate value for the latent heat of fusion (L_f). These quantities influence the nucleation rate in the classical calculation, which may be written (Pruppacher and Klett 1978)

$$J = 2N_c \left(\frac{\rho_w kT}{\rho_i h} \right) \left(\frac{\sigma_{i-w}}{kT} \right)^{1/2} \exp \left(\frac{-\Delta F_{\text{act}}}{kT} \right) \times \exp \left[\frac{-16\pi\sigma_{i-w}^3}{3kT(L_f\rho_i \ln(T_0 T^{-1}))^2} \right] \quad (3)$$

where N_c is the number of monomer molecules adjacent to a critical embryo, ρ_i is ice density, ρ_w is water

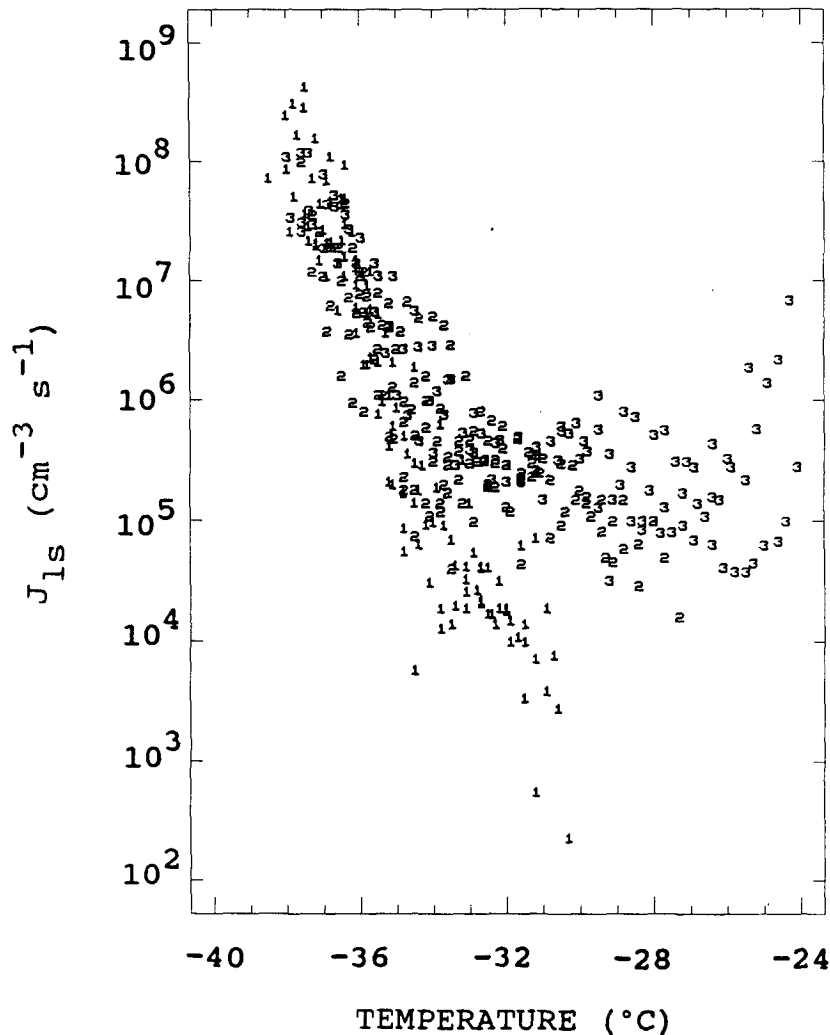


FIG. 8. Comparison of results for J_{1s} from Fig. 6 (1) and results after slight heterogeneous contamination of clouds (2), and in clouds formed on only slightly soluble carbonaceous soot particles (3).

density, T is temperature in $^{\circ}\text{K}$, T_0 is temperature at the melting point, and h and k are Planck's and Boltzmann's constants, respectively.

Nucleation rate is particularly sensitive to σ_{i-w} . To demonstrate this, we assume the temperature dependence for ΔF_{act} as given in Pruppacher and Klett, and we choose ρ_i , ρ_w , and L_f values to be average values over the supercooling, with temperature dependence also as given in Pruppacher and Klett. The results over the temperature range of our experiments and for a range of σ_{i-w} values are shown by the solid curves in Fig. 7. A constant value of $\sigma_{i-w} \approx 22.5$ characterizes most of the data, although a temperature dependence is noted. If this temperature dependence is considered, then $\sigma_{i-w} = 28.6 + 0.167T(^{\circ}\text{C})$ characterizes the results well, using data from below -34°C . Taborek (1985), Butorin and Skripov (1972) estimated characteristic values for σ_{i-w} of 28.6 and 28.3, respectively, over the

same temperature range as our results, but these authors assumed L_f to be constant at its value at 0°C , and they assumed ΔF_{act} to be constant with temperature (Taborek gives this a value of 3.4×10^{-13} ergs). Under these assumptions, a value for σ_{i-w} of 27.2 can characterize our results (see dashed curves in Fig. 6).

4. Summary

Estimates of the freezing rate of cloud droplets were made in simulations of the natural formation, growth, and cooling of an air parcel containing only CCN particles of soluble salt. Nucleation appears to be by homogeneous-freezing nucleation of the dilute solution droplets. Warmer than about -32°C , heterogeneous contamination produced clearly different results. Colder than -34°C , all results were dominated by the homogeneous-freezing process. The nucleation rate

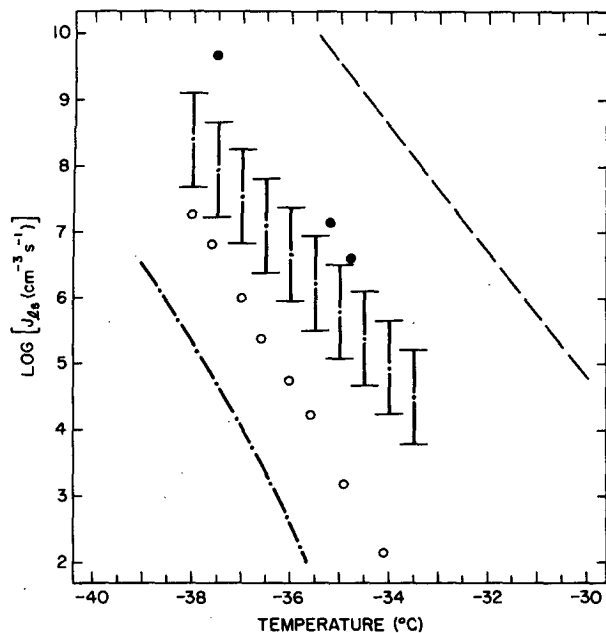


FIG. 9. Average J_k versus temperature from this study is plotted (with uncertainties given by bars) for comparison with results extrapolated from Hagen et al. (1981) (---), from Sassen and Dodd (1988) (●), from Butorin and Skripov (1972) (O), and from theoretical homogeneous-freezing nucleation (Pruppacher and Klett 1978) (—●—).

estimates are limited by experimental uncertainties in measured quantities and the dispersive nature of the clouds simulated. However, these experiments are some of the first realistic simulations of very cold cloud formation and freezing as it might occur in an ice nuclei scarce atmosphere. These results compared reasonably well with J_k derived from natural cloud studies.

Acknowledgments. This research was sponsored by USAF contract F33657-86-C-3002 and the National Science Foundation Grants ATM-8813345, ATM-8704776 and ATM-8519370. Special thanks to Mrs. Lucy McCall for drafting the figures.

REFERENCES

- Baumgardner, D., W. Strapp and J. E. Dye, 1985: Evaluation of the forward scattering spectrometer probe. Part II: Corrections for coincidence and dead-time losses. *J. Atmos. Oceanic Technol.*, **2**, 636–643.
- Butorin, G. T., and V. P. Skripov, 1972: Crystallization of supercooled water. *Kristallografiya*, **17**, 379–384.
- Cerni, T. A., 1983: Determination of the size and concentration of cloud drops with an FSSP. *J. Climate Appl. Meteor.*, **22**, 1346–1355.
- Cooper, W. A., 1988: Effects of coincidence on measurements with a Forward Scattering Spectrometer Probe. *J. Atmos. Oceanic Technol.*, **5**, 823–832.
- DeMott, P. J., 1988: Comparisons of the behavior of AgI-type ice nucleating aerosols in laboratory-simulated clouds. *J. Wea. Mod.*, **20**, 44–50.
- , 1990: Exploratory studies of condensation and ice nucleation by soot aerosols. *J. Appl. Meteor.*, submitted.
- Dye, J. E., and D. Baumgardner, 1985: Evaluation of the forward scattering spectrometer probe. Part I: Electronic and optical studies. *J. Atmos. Oceanic Technol.*, **1**, 329–344.
- Hagen, D. E., R. J. Anderson and J. L. Kassner, Jr., 1981: Homogeneous condensation freezing measurements for small water droplets in an expansion cloud chamber. *J. Atmos. Sci.*, **38**, 1236–1243.
- Heymsfield, A. J., and R. M. Sabin, 1989: Cirrus crystal nucleation by homogeneous freezing of solution droplets. *J. Atmos. Sci.*, **46**, 2252–2264.
- Lawson, R. P., and R. A. Stewart, 1983: An improved optical ice particle counter. *5th Symp. Meteor. Obs. and Instr.*, 11–15 April, Toronto, Canada, 46–53.
- Mage, D. T., and J. Noghrey, 1972: True atmospheric pollutant levels by use of transfer function for an analyzer system. *J. Air Poll. Control Assoc.*, **22**, 115–118.
- Pinnick, R. G., and H. J. Auvermann, 1979: Response characteristics of Knollenberg light-scattering aerosol counters. *J. Aerosol. Sci.*, **10**, 55–74.
- Pruppacher, H. R., and M. Neuberger, 1963: The effect of water soluble substances on the supercooling of water drops. *J. Atmos. Sci.*, **20**, 376–385.
- , and J. D. Klett, *Microphysics of Clouds and Precipitation*. D. Reidel, New York, 1978, 714 pp.
- Rogers, D. C., and G. Vali, 1987: Ice crystal production by mountain surfaces. *J. Climate Appl. Meteor.*, **29**, 1152–1168.
- Sassen, K., and G. C. Dodd, 1988: Homogeneous nucleation rate for highly supercooled cirrus cloud droplets. *J. Atmos. Sci.*, **45**, 1357–1369.
- Taborek, P., 1985: Nucleation in emulsified supercooled water. *Phys. Rev.*, **32**, 5902–5906.